SP2016_3125270

MIGRATION OF CENTER OF GRAVITY ON THE 40 INCH DIAMETER TANK WITH STIFFENING RINGS

J. Faure [(1)], J. Sargent [(2)], H. Gutierrez [(3)], D. Kirk [(4)], and W. Tam [(5)]

[(1)(2)(3)(4)] Florida Institute of Technology, 150 W. University Blvd., Melbourne, FL 32901, jfaure@my.fit.edu [(1)], sargent.joseph@gmail.com [(2)], hgutier@fit.edu [(3)], dkirk@fit.edu [(4)]
[(5)] ATK Space Systems, Inc., 6033 E. Bandini Blvd, Commerce, CA 90040, walter.tam@orbitalatk.com

KEYWORDS: Diaphragm tanks, stiffening, center of gravity, migration, 3-D scanning, Kinect

ABSTRACT:

Infrared scanning provides a superior 3-D mesh and point cloud to accurately calculate the center of gravity and center of mass without disrupting the 40 inch diaphragm shape. Four stiffening rings were epoxied sequentially with scans measuring the diaphragm shape at 10% intervals of fill fractions as the tank was emptied. Calculations of tank center of gravity show a significant shift in the Z-axis center of gravity with stiffening compared to no rings present while X-axis and Y-axis show minimal relative distortion.

1. INTRODUCTION & MOTIVATION

1.1. Introduction

This report provides an overview and results of measuring the center of gravity migration of the ATK 40 inch diaphragm tank for different fill levels using stiffening rings. The method used was 3-D scanning using an array of infrared sensors. Migration of the CG (center of gravity) has a significant effect over the stability of a spacecraft. The elastomeric diaphragm material considered in this study has the same thickness for all tanks [1].

During transportation or while on the launch pad, the propellant tank can experience oscillations. If sloshing forces are large enough, diaphragm pull-out may occur, or rubbing of the diaphragm on itself or against the tank, which can lead to weakening or tearing of the diaphragm. Diaphragm rubbing is of particular concern in larger diameter tanks. This is the reason for the stiffening rings which are used to prevent an undesirable shape which causes rubbing. Another benefit of the diaphragm which cannot be determined in a static experiment is that the stiffening rings could be used to dampen slosh motion inside the propellant tank. CG migration can be estimated by tracking the shape of the diaphragm for different fill levels on the 40 inch diameter simulator tank.

1.2. Proposed Approach for Estimation of Center of Gravity Migration using 3-D Scanning

The 3-D scanner provides a 3-D map of the diaphragm surface. With the diaphragm thickness, and with the known CAD model of the tank, the mass distribution of the propellant can be found. This, coupled with the location of the fixed coordinate system, allows the center of gravity to be found. Since the density and gravity are evenly distributed, the center of gravity, center of mass, and centroid of the tank are the same. This method also shows the shape of the diaphragm which can also show its behavior for different fill levels. This is ideal to identify rubbing visually, since using an LVDT (Linear Variable Differential Transformer) or strain gauges on the diaphragm surface cannot be used for this kind of detail. Also the nature of the 3-D scanner allows readings to be taken without any outside interference.

2. DESCRIPTION OF TEST APPARATUS

2.1. 3-D Scanner Test Rig

The scanner test rig includes six infrared cameras mounted around the tank, two groups of cameras ≈120° apart from one another. One group has cameras at a lower height and another group at a higher height in order to get a better perspective as seen in Figure 1. The frame below the tank is the tank stand built at Florida Tech to support the 40 inch tank.

Figure 1. 3-D scanning test rig on the 40 inch simulator tank

The tank stand seen in **Error! Reference source not found.** allows for easier tank disassembly than the one created by NASA. Any time the 40 inch tank needs to be removed it requires the use of 4 or more people to dismantle the frame and insert the stiffening rings, then reassemble the tank. The NASA A-frame on the other hand which was used in the previous 40 inch tank simulator study would require suspension by forklift above the A-frame for assembly and disassembly. The advantage the NASA tank stand has over the FIT tank stand is that it can be rotated, and the air can be purged out of the propellant side of the diaphragm using this feature. The FIT tank stand does not allow purging of air pockets. This is minimized prior to filling by purging the lines of air thoroughly, then applying pressure to the pressurant side, then connect the propellant line. In the end, the air pockets only occupy the volume between the quick connect and the ball valve of the propellant side of the tank.

Figure 2. Test rig - Cartesian coordinate system for center of gravity

Each group of cameras is connected to one computer. The scans have 1 mm accuracy (relative to the true 3-D shape) except at the edges of the scanned object (See previous Technical Report). The scans have two components: a standard 2D image, and an infrared depth scan. KScan3D is the scanning software that takes the scans, and aligns multiple cameras or one camera at different locations. The scans are combined and further aligned to one another on one computer. The scans can be edited, and finalized into one mesh which can be exported to another program.

Rhino is a CAD program that takes the surface profile and combines it with the CAD geometry of the lower tank wall. The diaphragm surface is further rendered in RhinoResurf, and then combined with the tank wall. The closed surface is then converted to a solid. The Rhino software can directly be used to determine the center of gravity in a separate coordinate system. The CAD model of the liquid propellant in the tank is treated as a solid, and the coordinate system matches the one seen in Figure 2.

2.2. Stiffening Ring Configuration

The diaphragm is fitted in the 40 inch tank simulator, and is airtight. Ring 0 is the standard diaphragm without any stiffening rings installed. The stiffening ring installation is cumulative starting from outside and moving inwards as seen in **Error! Reference source not found.** Ring 3 configuration for example includes Rings 1 through 3.

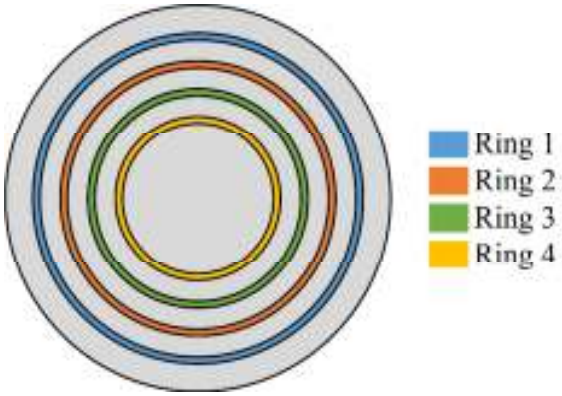

Figure 3. Stiffening Ring configuration

The thickness of the diaphragm material is 1.9133 mm (used for surface offset in Rhino). The distance between inner and outer radius for all stiffening rings is 1 inch.

Table 1. Stiffening Ring Placement

Ring Configuration	Outer Radius (in)
1	25.5
2	20.5
3	16.0
4	8.5

The 3-D scanner rig installed on the 40 inch tank is shown in Figure 4. The Kinect cameras take depth samples of the diaphragm. The data is further combined into one CAD model.

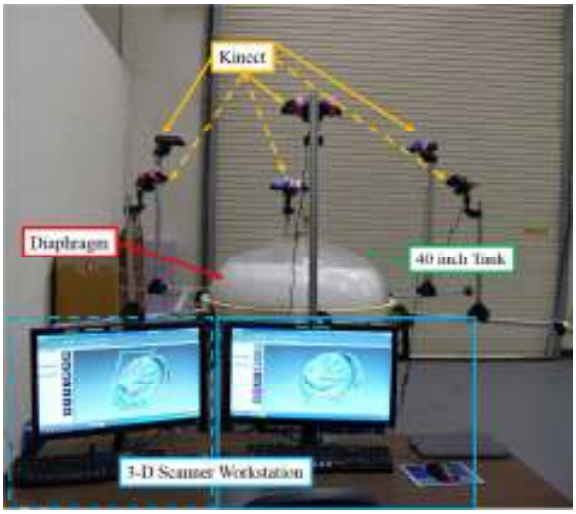

Figure 4. 3-D Scanning Test Rig using six Microsoft Kinect sensors.

2.3. Microsoft Kinect

The Kinect 1 sensor, as seen in the cut away view in **Error! Reference source not found.**, contains the following [2]:

1. RGB Color camera, similar to any web camera
2. Infrared emitter and an IR depth sensor
3. Multi-array microphone – four microphones for capturing sound
4. 3-axis accelerometer – configured for a 2 gravity range to determine the current orientation of the Kinect.

The effective vertical range is 43° ±27°, and the horizontal range is 57° [3]. The resolution of the RGB color camera is 640x480 pixels at 30 frames per second [2]. The depth resolution by the IR emitter and depth sensor is <1mm with a range of 300-1500 mm. The IR emitter projects an irregular pattern of IR dots of varying intensities. The IR camera reconstructs a depth image by recognizing the distortion in the pattern. Kinect works using a stereo matching algorithm. It captures stereo with only one camera [2].

When using multiple Kinect sensors to create a 3-D point cloud, interference is caused by the other IR emitters. Interference increases as the number of Kinects increases.

Interference can be reduced through multiple methods: Vibration, mechanical shutter, and disabling the IR emitter. Vibration reduces the noise by moving the IR patterns out of phase. Our Kinects have been mounted on individual vibration systems, based on a DC motor that rotates at a specific frequency as seen in Figure 5. Figure 6 shows the depth image with and without vibration.

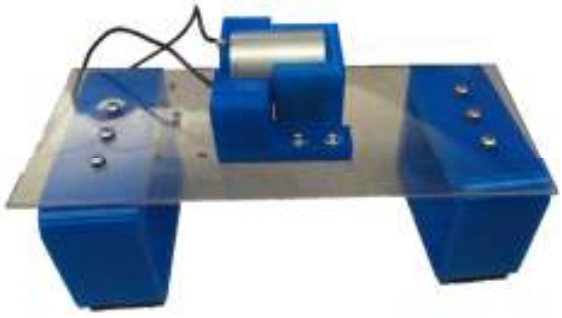

Figure 5. Vibration system [1]

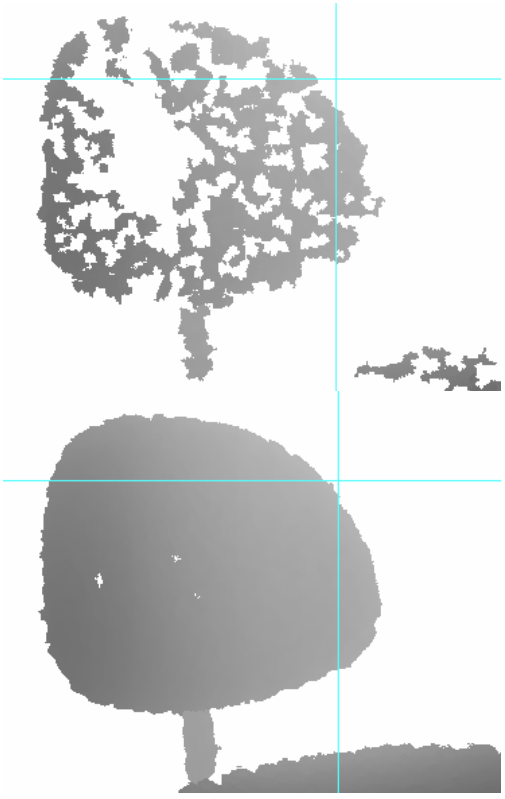

Figure 6. Depth image of a chair without (top) and with (bottom) the vibration system on [1]

An alternative method to avoid interference is shutting off the IR emitters via software and call the emitter only when needed in sequence, engaging or disengaging the IR emitters in precise intervals. This method is used for the static tests and considerably reduces interference because only one camera need be ON at any given time. For dynamic testing, the vibration method is the only viable way of reducing noise. The Kinect stereovision cameras uses ≈ 65% of the USB 2.0 controller bandwidth, and require separate USB cards since there are no more separate controllers available on the motherboard. The hardware setup based on extruded beams, 3-D printed vibration motor mounts, Panvise supports, 3-D printed sliding mounts and anchor is shown in **Error! Reference source not found.**9.

2.4. KScan3D

KScan3D is a software that can take a maximum of 4 Kinects per computer. This program can scan with multiple Kinects, align, generate mesh, combine meshes, delete various vertex points and finalize the mesh. Alignment is done by aligning the vertex points together. The scans are finalized into a mesh where detail, and hole filling are used. Hole filling enables gaps in the mesh to close up. These files then can be output into a format that can be used in another application.

2.5. MATLAB

MATLAB is used to control KScan3D for capture purposes only, as seen in Figure 7. A MATLAB script operates the KScan on both computers, engaging one Kinect IR emitter at a given time to reduce interference and moves in sequence first one computer, then the second computer and in each computer it moves from the first to the last Kinect. Then it reengages the IR emitters. Figure 7 shows only one workstation linked. This GUI can work with either one or both workstations.

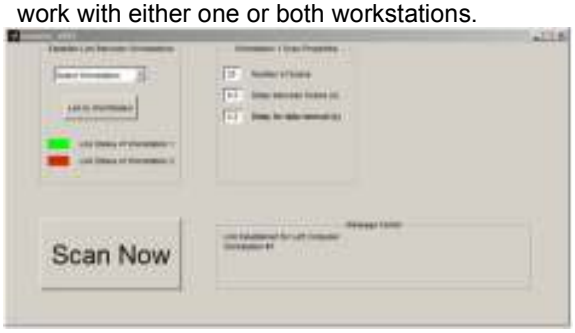

Figure 7. MATLAB Capture Scan GUI across two computers developed at Florida Tech

MATLAB is also used to reduce the time spent in post processing in Rhino by importing the object file from Kscan3D. The file is then aligned so the top of the aluminum surface is parallel with the x-y plane. Then the x-y center is located on the Plexiglas flange outer surface based on 3 points of a circle. This is interpolated from a range between the top of both Plexiglas and aluminum flanges, 2 centimeters above the aluminum flange points. The z-coordinates are obtained, and averaged to set the z-position zero. This takes the user approximately 15 minutes to complete in CAD. Manually setting the orientation and zero for x-y-z coordinates can take a couple of hours when done carefully.

Figure 8. Sequence scanned by each computer

2.6. Rhino

Rhino 5 with RhinoResurf is used to clean up meshes by converting polygons in a mesh into a surface. This allows the file size to be smaller and has no holes, and the interpolation is very good [1]. Splicing the tank wall and the diaphragm surface together is followed by offsetting the surface by the diaphragm thickness. The next step is to blend any open surfaces, and generate a solid object ("closed poly surface") see Figure 9. Rhino has the

capability to generate moments of inertia, centroid, and volume.

Figure 9. Real shape (left) and after surfacing (right) [1]

2.7. Sources of Error

The main source of error in the 3-D scanner is given by how much the shape is affected by optical distortions, image noise in the cameras and the methods used for manipulation of the scan data.

The 3-D scanner is susceptible to optical distortions of the tank wall. The distortions increase at higher sensor pitch angles, so the cameras must be either mounted close to the flange with a low pitch angle or further away at a higher pitch angle. The maximum depth range is 1.5 meters, so there are limitations to the distance the camera can move from the test rig. The 3-D scanner takes a series of depth data (50 points per camera for the static test) and overlays them. There is some uncertainty in the mesh generated, but less than 1 mm.

The data is then combined and finalized into a single mesh. The mesh is then imported and smoothed out by RhinoResurf, which includes further interpolation. Then the surface is offset uniformly by the diaphragm thickness, and is further combined with the CAD tank geometry, and merged to form a solid for center of gravity analysis. The uniform offset will distort the results but marginally, since the offset thickness is 1.9133 mm above the diaphragm on the pressurant side of the tank. Considering the volume of the tank even at the lowest (80 liters), the volume of the stiffening rings is negligible by comparison for all rings the volume taken is less than 0.6L. The tank, and diaphragm orientation was consistently placed on the same floor location due to markings varying by no more than $1/16^{th}$ of an inch. The pitch and yaw orientation with respect to the tank was within 1 degree of vertical.

3. RESULTS

3.1. Center of Gravity Location

There are no existing drawings or a CAD model of the simulator tank. During filling the estimated total volume is 445 Liters (16 Liters less than on our approximated CAD model). A scan at an empty fill level is used to estimate the geometry of the bottom portion of the tank (from the top of the aluminum flange down to the diaphragm).

The center of gravity locations were estimated by 3-D Scanner by the procedure outlined above, for ten fill levels. The results for x-y centers of gravity are shown in Table 2 and Table 3.

There is some difference between the first stiffening rings and the remaining cases (rings: 0, 2, 3, 4). Ring 1 configuration has the lowest x-y center of gravity locations, roughly 1 inch less in the x-direction across the board in Table 2, and ½ inch less in the y-direction across the board in Table 3.

Table 2: 40 inch Tank: X-Center of Gravity Migration for ten fill levels for each stiffening configuration

Fill Volume (L)	x_0 (in)	x_1 (in)	x_2 (in)	x_3 (in)	x_4 (in)
395.36	32.08	32.62	32.56	32.58	32.64
360.36	32.59	31.77	32.58	32.67	32.55
325.36	32.61	31.72	32.35	32.46	32.48
290.36	32.62	31.66	32.48	32.54	32.56
255.36	32.66	31.40	32.53	32.64	32.71
220.36	32.64	31.45	32.48	32.57	32.80
185.36	31.90	31.41	32.60	32.62	32.43
150.36	31.86	31.53	32.23	32.50	32.25
115.36	32.31	31.12	32.28	32.09	31.85
80.36	32.79	31.12	32.07	32.70	32.82

Table 3: 40 inch Tank: Y-Center of Gravity Migration for ten fill levels for each stiffening configuration

Fill Volume (L)	y_0 (in)	y_1 (in)	y_2 (in)	y_3 (in)	y_4 (in)
395.36	31.73	32.94	33.00	32.90	32.92
360.36	32.90	32.66	32.93	32.92	32.97
325.36	32.92	32.48	32.89	33.04	33.01
290.36	33.15	32.63	33.03	32.98	33.06
255.36	33.11	32.66	33.02	33.01	33.14
220.36	33.21	32.56	33.23	33.10	33.23
185.36	33.27	32.70	33.50	33.37	33.29
150.36	33.13	32.25	33.44	33.25	33.09
115.36	33.23	32.54	33.38	33.22	33.57
80.36	33.41	32.29	33.33	33.84	33.44

The z-center of gravity position shown in Table 4 follow a similar trend for all non-zero ring configurations. Ring configuration 1-4 follow the same trends as Ring configuration 0 between100-60% fill level or 395L-255L fill volume. For fill volumes with 220L and below the difference between Ring configuration 0 and Ring configuration 1-4 becomes apparent, approaching 1 inch.

Table 4: 40 inch Tank: Z-Center of Gravity Migration for ten fill levels for each stiffening configuration

Fill Volume (L)	z_0 (in)	z_1 (in)	z_2 (in)	z_3 (in)	z_4 (in)
395.36	-1.81	-1.74	-1.80	-1.89	-2.03
360.36	-2.84	-2.96	-2.69	-2.89	-3.02
325.36	-3.73	-4.31	-3.62	-3.88	-3.96
290.36	-4.74	-4.64	-4.55	-4.69	-4.81
255.36	-5.74	-5.51	-5.42	-5.56	-5.67
220.36	-7.04	-6.38	-6.27	-6.36	-6.41
185.36	-7.96	-7.15	-7.17	-7.30	-7.38
150.36	-8.39	-7.97	-7.97	-8.04	-8.14
115.36	-9.53	-8.60	-8.71	-8.70	-8.91
80.36	-10.61	-9.53	-9.33	-9.15	-9.70

Figure 10 shows the Center of Gravity migration as fill level changes. The trends for the x center of gravity position shows a general scatter within 1 inch across all fill volumes. The exception is the Ring 1 configuration which shows a lower center of gravity than the rest of the configurations. Ring configurations 1-4 have the same starting point at 395L, but diverge at the next fill volume of 360L. The general trend for the y center of gravity position increases with a higher fill volume, but it does not vary significantly for all ring configurations with the exception of Ring 1. Similar to the x-center of gravity positions Ring 1 has a lower y center of gravity position. Ring configurations 1-4 have the same starting point at 395L, but diverge from each other at the next fill volume. Both x-y center of gravity positions have different positions for Ring 0 than Ring 1-4 at 395L. The trends for the z center of gravity position shows a decreasing linear trend across all fill volumes with little difference between each configuration.

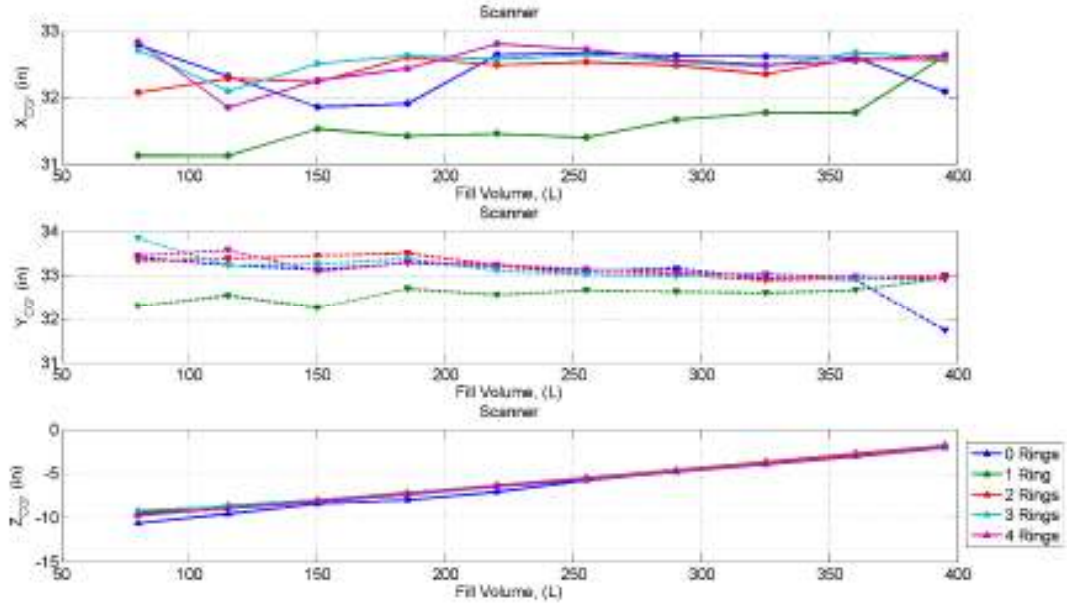

Figure 10. Migration of CG coordinates (X,Y,Z) as function of fill Level

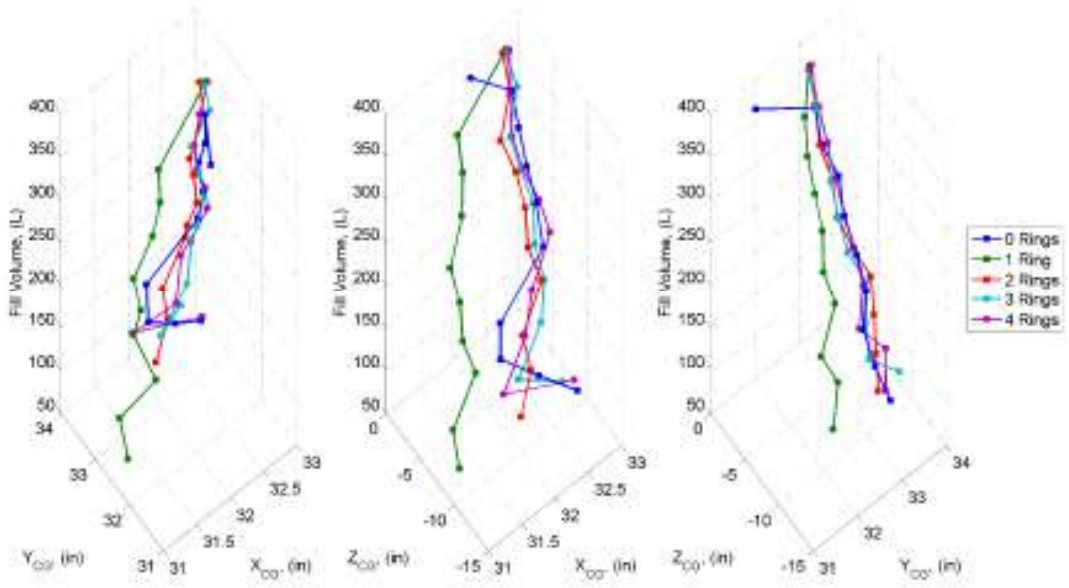

Figure 11. Migration of CG coordinates as a function of fill level

Figure 11 shows the spatial relationship between each plane (X-Y, X-Z, Y-Z) and fill level in 3-D space. In the Y-Z subplot, the relationship between volume and Y-Z is nearly linear. The X-Y and X-Z subplots both show noise in the x-direction, but the y and z linear relationships are more apparent with fill volume.

The Ring 0 configuration (no ring) is used as reference for all percent difference calculations. As seen in Figure 11 Ring 1 has the lowest x-y center of gravity positions of the 5 configurations so the percent difference will always be comparatively higher. Figure 12 and Figure 13 shows very little variation for Ring configurations 2-4 when

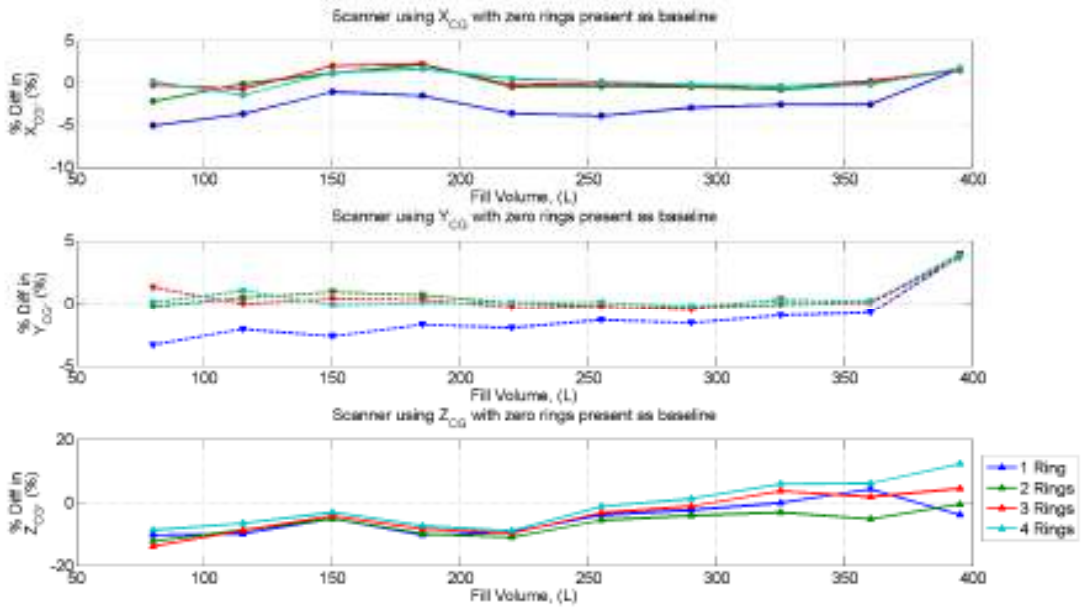

Figure 12. Percent difference of center of gravity for Ring configuration 1-4 compared to Ring 0

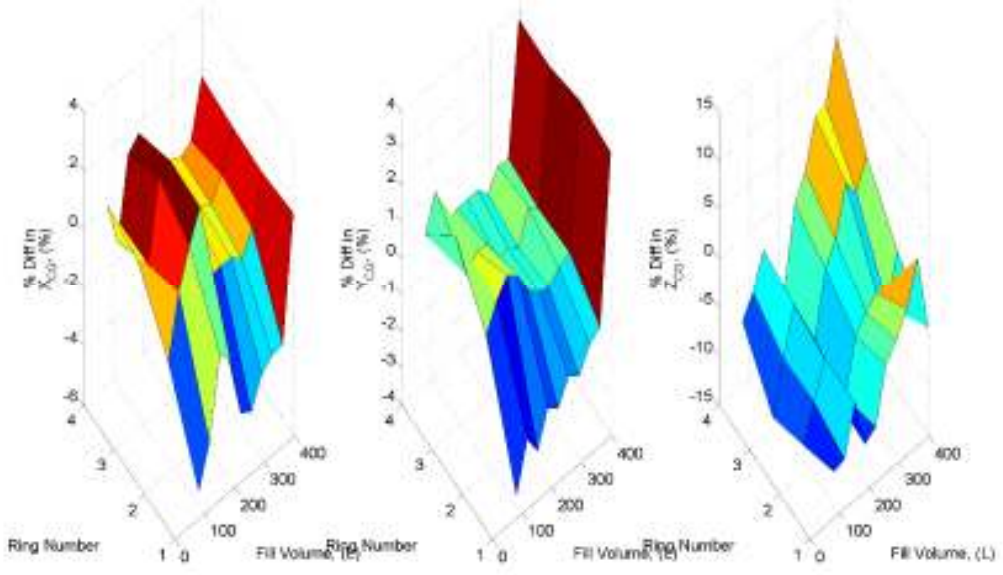

Figure 13. Percent difference of center of gravity as a surface using Ring 0 as reference

compared to Ring 0. Figure 13 shows the same trends as Figure 12 except it integrates the ring configuration as a dependent variable. The exception is the fill volume of 395L where the differences of Ring 1-4 have a slightly higher value than Ring 0. In the percent difference in the z-direction excluding Ring 1 for the most part (fill volumes 255L-395L), the percent difference increases with a higher ring configuration. The reverse of this trend is true for fill volumes less than 255L. It should also be noted that the percent difference between Rings 1-4 converge at 255L and continue to 80L.

3.2. Rendered Diaphragm Profiles for Each Fill Fraction

Figure 14 to Figure 16 show the corresponding diaphragm profiles for several fill fractions for each ring configuration.

As can be seen in Figure 14, the variation between Ring 1-3 is less than between 3-4. In Figure 15, there are dimples in the diaphragm surface in Ring 0, with Ring 1-4 the dimples are no longer present. Similar effects can be seen in Figure 16, however the rings obviously reduce rubbing of the diaphragm wall on itself on the outside. However, on the inside of diaphragm surface the diaphragm begins to rub against itself with more rings. Generally speaking Ring 2 configuration yields the 'best of both worlds' where it reduces the dimples on both outside and inside. Bear in mind there are air pockets present, and the stiffening rings may

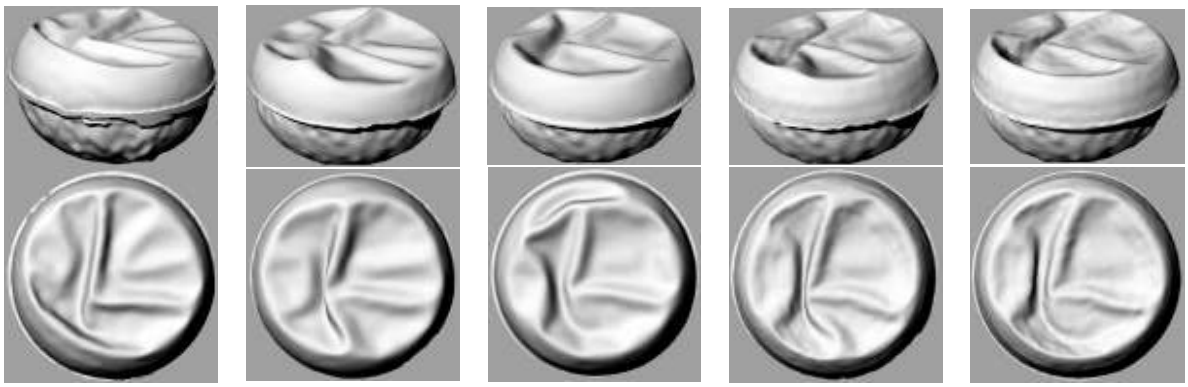

Figure 14. Scan isometric View (top), and Top View (bottom), fill level = 395L

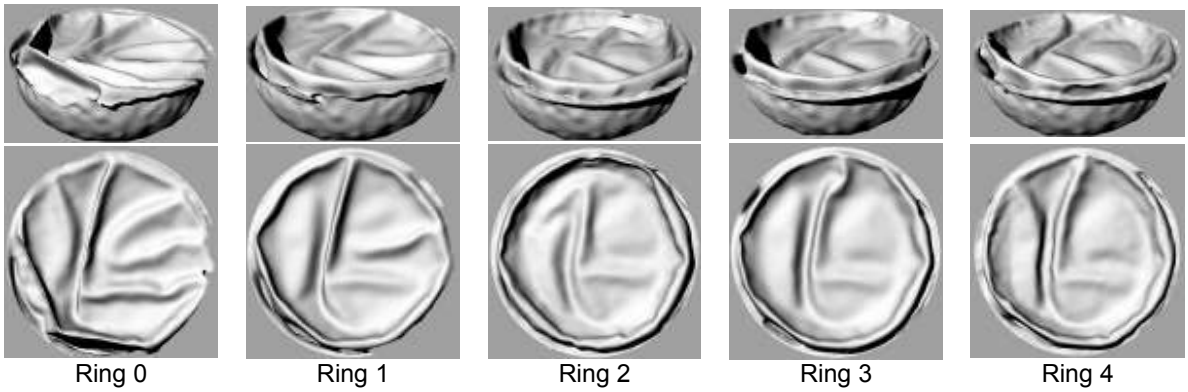

Figure 15. Scan isometric View (top), and Top View (bottom), fill level = 255L

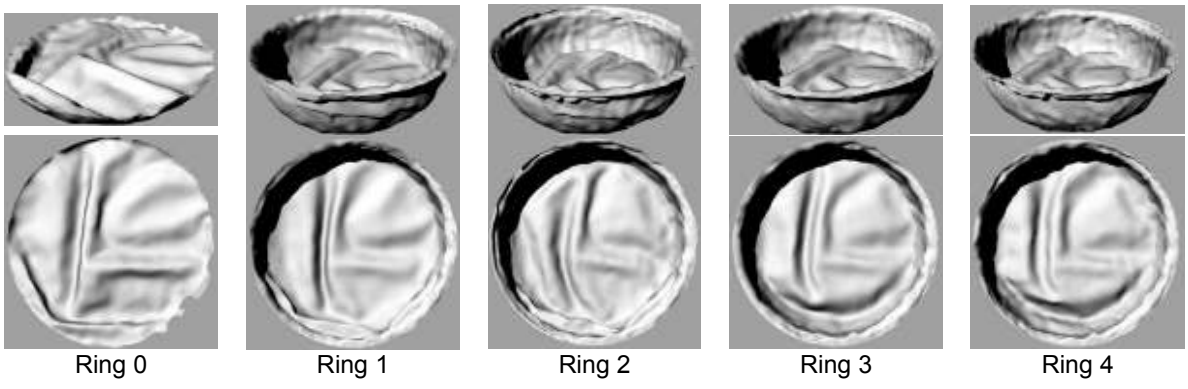

Figure 16. Scan isometric View (top), and Top View (bottom), fill level = 80L

amplify the effect of rubbing with a higher ring number. The propensity of rubbing is still present with a high ring number, but to a less degree with the propellant side being filled with liquid.

4. CONCLUSIONS

Results are presented that show the CG migration of the 40 inch simulator tank as function of fill level with stiffening rings. The 3-D scanner provides a direct estimate of the shape of the diaphragm, which is later integrated in Computer Aided Drawing software to provide an estimate of the CG location. Accuracy and resolution of the 3-D scanner method was estimated by comparing scanning results of 3-D printed models of known geometries to their corresponding CAD models, as discussed on a previous report. The scanning method for estimation of 3-D surface geometry was shown to be accurate within the accuracy of the depth sensors (better than 1 mm), and unlike the LVDT method, it was not limited to estimate CG location in the X-Y direction but also in Z. The scanner is not susceptible to lateral force effects at the tank's support points, as is the case in the LVDT method.

There was a linear trend between fill level and z-center of gravity position. The x-center of gravity location had less variation than the y-center of gravity location. The stiffening rings had an effect on the center of gravity in the x and y directions, but less of an effect in the z direction. Adding a single ring has an effect on the shape of the diaphragm. A balance of the number of Rings in this case two rings seems to offer the best reduction of diaphragm rubbing as fill level decreases.

Care must be taken so that the infrared scanner cameras have a proper view of the tank, and their elevation angle is sufficiently low to minimize optical distortion.

5. REFERNCES

[1] M. Bouyssou, "3-D scanning for surface characterization based on circular array of Kinect," ENSMM, Melbourne, 2014.

[2] P. P. Das, "Kinectic vision looking deep into depth," 18 12 2013. [Online]. Available: http://www.slideshare.net/ppd1961/kinectic-vision-looking-deep-into-depth. [Accessed January 2014].

[3] Microsoft, "Kinect for Windows Sensor Components and Specifications," Microsoft, [Online]. Available: http://msdn.microsoft.com/en-us/library/jj131033.aspx. [Accessed 5 2014].